Epstein, J. S. Miller, *Science* **252**, 1415 (1991).
7. K. Itaya, I. Uchida, V. D. Neff, *Acc. Chem. Res.* **19**, 162 (1986).
8. The cyanochromate $[Cr_5(CN)_{12}] \cdot 10H_2O$ with T_c = 240 K, reported by T. Mallah *et al.* (*4*), has the highest T_c reported for a stable molecular-based magnet before the present work.
9. $V(TCNE)_2 \cdot 0.5CH_2Cl_2$, reported by J. M. Manriquez *et al.* (*6*), shows spontaneous magnetization at room temperature but is air-sensitive. The T_c of 270 K obtained in the present study is the second highest T_c reported if such air-sensitive magnets are included in the comparison.
10. W. B. Schaap, R. Krishnamurthy, D. K. Wakefield, W. F. Coleman, in *Coordination Chemistry*, S. Kirschner, Ed. (Plenum, New York, 1969), pp. 177–206.
11. Elemental analysis of the three materials was as follows. (a): C, 17.57%; N, 20.50%; H, 2.97%; and Cr, 30.87%. (b): C, 22.32%; N, 25.65%; H, 1.72%; and Cr, 33.87%. (c): C, 14.98%; N, 16.50%; H, 0.73%; Cr, 21.71%; and Cs, 30.91%. Small amounts of K and Cl were also found in (c). The unit cell formulas of (a), (b), and (c) were $Cr^{II}_{3.61}Cr^{III}_{3.19}(CN)_{16.78}[\ ]_{1.20}(H_2O)_{17.03}$, $Cr^{II}_{1.29}Cr^{III}_{6.29}(CN)_{21.43}[\ ]_{0.43}(H_2O)_{10.00}$, and $Cs_{4.34}Cr^{II}_{5.02}Cr^{III}_{2.75}(CN)_{22.64}[\ ]_{0.23}(H_2O)_{6.72}$, respectively, where [ ] stands for $Cr(CN)_6$ vacancies. Considering the experimental error, the structures corresponding to (a) $\{Cr_{2.43}(CN)_6 = Cr^{II}_{1.29}Cr^{III}_{0.14}[Cr^{III}(CN)_6]\}$ and (c) $\{Cs_{1.15}Cr_{2.06}(CN)_6 = Cs_{1.15}Cr^{II}_{0.33}Cr^{III}_{0.73}[Cr^{II}(CN)_6]\}$ were qualitatively consistent with the typical structure $Cr_{2.5}(CN)_6 = Cr^{II}_{1.5}Cr^{III}(CN)_6$ [saturation magnetization expected is 3 μ_B per $Cr_{2.5}(CN)_6$] and $CsCr_2(CN)_6 = CsCr^{III}Cr^{II}(CN)_6$ [1 μ_B per $CsCr_2(CN)_6$], respectively. The error of the ratio of Cr to CN for the materials prepared under same electrochemical conditions was ±4% at maximum. The materials did not have as pure and well-defined a structure as would a single crystal.
12. K. Nakamoto, Ed., *Infrared and Raman Spectra of Inorganic and Coordination Compounds* (Wiley, New York, ed. 4, 1986).
13. The magnetizations at 5 T per unit cell of (a), (b), and (c) were 2.0, 1.8, and 2.6 μ_B, respectively, whereas the saturation magnetizations expected from these formulas were 7.2, 2.6, and 5.7 μ_B, respectively. The first magnetization curves at 10 K showed that magnetization for (b) almost saturated at 5 T. The saturation magnetization of (b), 1.8 μ_B per unit cell, was relatively close to the 2.6 μ_B expected from the unit cell formula. The low saturation magnetization could be explained by the existence of a relatively large amount of Cr^{III}-CN-Cr^{III} moieties, in which the spins of the *d* orbital canceled out each other. On the other hand, the magnetization curves for (a) and (c) still increased at around 5 T, and the magnetizations obtained at 5 T for (a) and (c) were fairly small compared with saturation magnetization expected from their formulas. However, it seems that such small values are often observed for chromium cyanide magnets. Mallah *et al.* (*4*), for example, reported 1.4 μ_B at 7 T, instead of the expected 6 μ_B, for $Cr_5(CN)_{12}$ (T_c = 240 K).
14. The FT-IR spectra obtained before and after the electrochemical reduction showed that the absorption coefficient of CN at 2071 cm^{-1} was about 1.7 times as large as that at 2187 cm^{-1}. Considering the relative absorption coefficient of the CN stretching peaks and the IR spectra in Fig. 2, the ratio of Cr^{III} to Cr^{II} coordinated to the carbon in (b) could be estimated to be 0.80:0.20, that is, $Cr^{II}_{0.16}$(high-spin)$Cr^{III}_{0.96}[Cr^{II}_{0.20}$(low-spin)$Cr^{III}_{0.80}(CN)_6]$.
15. Electrically tunable magnets are proposed here to be designated as "electromagnetic materials" by analogy with the term "electrochromism."
16. We thank H. Etoh and J. Ichiyanagi for their support in these experiments and D. Tryk for reading the manuscript.

22 May 1995; accepted 13 November 1995

Achieving Linear Scaling for the Electronic Quantum Coulomb Problem

Matthew C. Strain, Gustavo E. Scuseria,* Michael J. Frisch

The computation of the electron-electron Coulomb interaction is one of the limiting factors in ab initio electronic structure calculations. The computational requirements for calculating the Coulomb term with commonly used analytic integration techniques between Gaussian functions prohibit electronic structure calculations of large molecules and other nanosystems. Here, it is shown that a generalization of the fast multipole method to Gaussian charge distributions dramatically reduces the computational requirements of the electronic quantum Coulomb problem. Benchmark calculations on graphitic sheets containing more than 400 atoms show near linear scaling together with high speed and accuracy.

Although first-principles electronic structure calculations of molecules have become routine, they remain limited to systems of modest size because of their steep computational cost. The electronic Coulomb problem, which scales quadratically with system size, is one of the fundamental obstacles in the quest for ab initio computations of large molecules. In this report, we present quantitative evidence demonstrating that a generalization of the fast multipole method (FMM) (*1*–*3*) to Gaussian charge distributions achieves near-linear scaling for the quantum Coulomb problem. The method, the accuracy of which we have tuned to machine precision in specific cases, becomes faster than standard analytic evaluation of Gaussian two-electron integrals for systems containing as few as 300 basis functions. Our method integrates concepts recently introduced by others (*4*, *5*) with unique elements as described below.

In the FMM, the system under consideration is embedded in a hierarchy of 8^n ($n < 7$ in this work) cubic boxes at the finest mesh level, where n specifies the total number of tiers. All charge distributions located in a given box are represented by multipole expansions about the center of the box. For highly accurate results, the near-field (NF) portion of the problem, which is defined by interactions inside a given box and neighboring boxes, is treated exactly. Interactions in the far-field (FF) are treated through multipole expansions. The distinctive characteristic of the FMM is that translation techniques allow these multipole expansions to interact at different mesh levels (depending on the distance between their centers) through an upward and downward pass of the tree hierarchy, yielding a method with effective linear scaling (*2*).

Crucial to the generalization of the Greengard-Rohklin algorithm (*1*, *2*) to the quantum Coulomb problem is the definition of range or spatial extent of a continuum charge distribution. For Gaussian functions (*4*), the range definition can be derived from the basic Coulomb integral between two *s*-type distributions (*6*) as

$$r = (2s)^{-1/2}\,\mathrm{Erfc}^{-1}(\varepsilon) \qquad (1)$$

where s is the exponent of the product Gaussian distribution, Erfc^{-1} is the inverse of the complementary error function, and ε is the desired error in the approximation. The real number r is rounded up to the nearest integer, thus guaranteeing an error smaller than ε per interaction (*7*). In our Gaussian FMM (GFMM) implementation, a given interaction is included in the FF only if the number of boxes separating the edge of the boxes containing the two charge distributions is larger than the sum of the ranges of the distributions; for the results presented in this report, this number is at least two boxes. The electron-electron NF interactions were treated exactly through six-dimensional analytic integration of Gaussian functions. We also truncated the maximum l (l_{max}) of a given multipole expansion to an effective value l_{eff} based on

$$\varepsilon = k(a/R)^{l_{eff}} \qquad (2)$$

where ε is the desired accuracy, a is a constant whose optimum value is 0.63, and k is adjusted such that $l_{eff} = l_{max}$ when $R = 3$ boxes. This simple formula is straightforward, substantially improves the speed of the GFMM (which asymptotically scales as l^4_{max}), and still yields very accurate results. This approach, which shares the basic philosophy of the "very fast" FMM recently introduced for the point-charge case (*5*), is partially responsible for the good scaling properties of our method and is denoted GvFMM herein (*7*).

All computational developments and calculations reported here were carried out with a development version of the Gaussian suite

M. C. Strain and G. E. Scuseria, Center for Nanoscale Science and Technology, Rice Quantum Institute, and Department of Chemistry, MS 60, Rice University, Houston, TX 77005–1892, USA.
M. J. Frisch, Lorentzian, Inc., 140 Washington Avenue, North Haven, CT 06473, USA.

*To whom correspondence should be addressed.

of programs (8). The basis sets used in the benchmark calculations were 3-21G and 6-31G**. The latter consists of (4*s*2*p*1*d*)- and (2*s*1*p*)-contracted Gaussian functions for carbon and hydrogen, respectively. The graphitic sheets used in the benchmark calculations (9) consisted of the series of molecules $C_{6m^2}H_{6m}$ for m = 1 to 8. The Coulomb contribution to the Hamiltonian (Coulomb matrix) and Coulomb energies were obtained with the use of the tight self-consistent field (SCF) option of the Gaussian program (8). Total energies were evaluated at the local density approximation (LDA) of density functional theory with the fine-grid option in the same package.

Table 1 presents a selection of representative total energy errors using two sets of parameters: the set l_{max} = 15 and $\varepsilon = 10^{-9}$, for demonstrating the accuracy of the method, and the set l_{max} = 12 and $\varepsilon = 10^{-6}$, which was used in the rest of the calculations reported here. The latter set provides the desired accuracy of $\sim 10^{-6}$ Hartrees for the Coulomb energy, which is smaller than the estimated numerical error arising from the exchange-correlation numerical quadrature, and should have a negligible effect on the chemistry under study.

The number of significant charge distributions (products of basis functions) depends linearly on the number of contracted Gaussian basis functions for the two different bases studied (Fig. 1). Negligible charge distributions were eliminated by the existing orbital-pair screening tools in the Gaussian program (8); such screening is a prerequisite for achieving linear scaling for the Coulomb problem.

We compared the computational (CPU) times required for calculating the entire (NF + FF) Coulomb matrix with standard analytic two-electron integral evaluation between contracted Gaussian functions and with GvFMM (Fig. 2). The GvFMM becomes competitive with analytic integration for modest system size ($C_{24}H_{12}$ in Fig. 2) and a small number of basis functions ($\sim$300). If the three points corresponding to the largest calculations on each of the curves in Fig. 2 are fitted with an N^{Ω} functional form, we obtain an effective scaling exponent of Ω = 2.11 for analytic integration [in agreement with our previous estimate (9) based on a different integral package] and Ω = 1.35 for the GvFMM. The asymptotic scaling exponent for the GvFMM is thus substantially lower than the limiting quadratic behavior observed for analytic integration. For the largest calculation carried out in this work, $C_{384}H_{48}$ with a 3-21G basis, the GvFMM is more than eight times faster than analytic integration (Fig. 2). This is accomplished in calculations with an accuracy of $\sim 10^{-6}$ Hartrees.

The computational cost of the FF portion of the Coulomb problem was determined as a function of molecular size for different numbers of boxes and values of l_{max} (Fig. 3). Sublinear and near-linear scaling behavior is evident from these data. If for a fixed number of boxes the molecular system increases in size, the box length increases and the Gaussian ranges decrease, until eventually they all reach a range of 1 box, at which point the scaling becomes quadratic. However, our benchmarks indicate that faster execution of the entire Coulomb problem (NF + FF) using one more tier occurs well before the limiting case of range 1 box. Thus, quadratic scaling in the GvFMM is avoided in a manner similar to that of the point-charge case (2).

A breakdown of the NF and FF components of the Coulomb problem calculated with the GvFMM for 8^5 boxes (Fig. 4) shows that the computational time is dominated by the NF portion of the problem (that is, analytic integration of the interactions not picked up by the GFMM), even though the vast majority of interactions occur in the FF. For $C_{384}H_{48}$ in a 3-21G basis, 97% of all interactions are in the FF, and $\sim$50% of the remaining 3% NF inte-

Table 1. Energy errors between exact and GvFMM Coulomb energies.

Molecule	Basis set	Number of boxes	Number of distributions	Absolute error (Hartrees)
		$\varepsilon = 10^{-9}$, l_{max} = 15		
C_6H_6	6-31G**	8^3	2,949	3.7×10^{-10}
$C_{24}H_{12}$	6-31G**	8^3	17,289	3.2×10^{-9}
$C_{54}H_{18}$	6-31G**	8^4	43,515	5.0×10^{-9}
		$\varepsilon = 10^{-6}$, l_{max} = 12		
$C_{96}H_{24}$	3-21G	8^5	30,021	6.8×10^{-6}
$C_{150}H_{30}$	3-21G	8^5	48,063	9.7×10^{-6}
$C_{216}H_{36}$	3-21G	8^5	70,281	5.6×10^{-6}
$C_{294}H_{42}$	3-21G	8^5	96,675	2.9×10^{-6}
$C_{384}H_{48}$	3-21G	8^5	127,245	9.1×10^{-6}

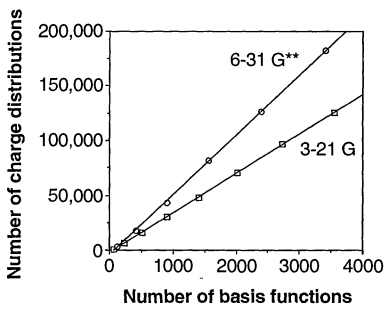

Fig. 1. Linear dependence of the number of non-negligible charge distributions on the number of contracted Gaussian functions in $C_{6m^2}H_{6m}$ (m = 1 to 8) graphitic sheets obtained with existing orbital-pair screening tools in the Gaussian program.

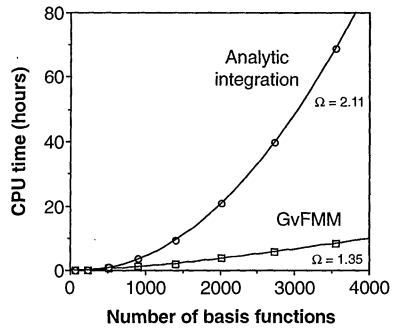

Fig. 2. CPU times (obtained on an IBM/RS6000-370) for the formation of the Coulomb matrix (first iteration of the SCF procedure), in a series of $C_{6m^2}H_{6m}$ (m = 1 to 8) graphitic sheets with a 3-21G basis, for state-of-the-art analytic integration of contracted Gaussian functions and for GvFMM with 8^3 (m = 1), 8^4 (m = 2), 8^5 (m = 3 to 7), and 8^6 (m = 8) boxes. The Ω parameter is the asymptotic scaling exponent (time $\sim N^{\Omega}$) obtained in a log-log plot of the three largest calculations for both curves. The crossover between the two curves occurs at approximately 300 basis functions.

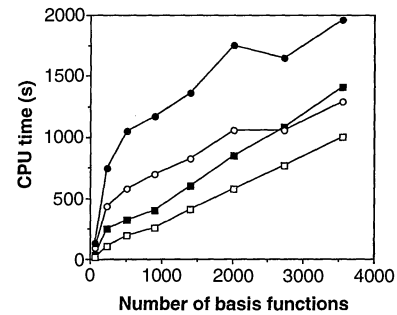

Fig. 3. Near-linear CPU time (obtained on an IBM/RS6000-370) dependence of the far-field (FF) component of the molecular Coulomb problem on the number of contracted Gaussian functions. Cusps on the curves result from changes in Gaussian ranges with increasing size of the graphitic sheets. From top to bottom: (●) 8^5 boxes, l_{max} = 15; (○) 8^5 boxes, l_{max} = 12; (■) 8^4 boxes, l_{max} = 15; and (□) 8^4 boxes, l_{max} = 12.

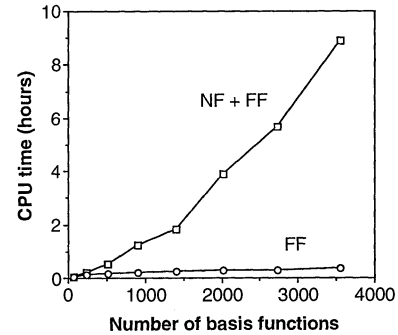

Fig. 4. CPU times (obtained on an IBM/RS6000-370) for computing the NF and FF components of the quantum Coulomb problem in a series of graphitic sheets with a 3-21G basis and 8^5 boxes. Note the relatively large computational cost of the NF component, even though for the largest systems, the FF accounts for more than 95% of all interactions.

grals are neglected as a result of the screening techniques (Fig. 5). Thus, a mere ~1.5% of all interactions in this molecule are treated by analytic integration. However, this computation is costly (Fig. 4).

In the GFMM, the separation between NF and FF is done in terms of uncontracted Gaussian functions because the product of two contracted Gaussians gives a linear combination of Gaussian distributions with different exponents centered at different points. The range criterion explained above thus has to be individually applied to these charge distributions. On the other hand, modern Gaussian integral packages, and in particular the PRISM algorithm (*10*) used in the Gaussian program (8), utilize contracted basis sets, thereby significantly reducing the computational cost of evaluating integrals over the uncontracted set. We estimate (Figs. 4 and 5) that calculating NF integrals over uncontracted rather than contracted functions for the 3-21G basis increases the computational cost by a factor of 5. This factor imposes a lower bound on the percentage of interactions that must be included in the FF for the GvFMM to become competitive with analytic integration. Given an overhead factor of 5 and neglecting the cost of FF evaluation, the GvFMM would be more expensive than analytic integration whenever more than 20% of all interactions were included in the NF. In our benchmarks, this break-even point is achieved at small molecular size (Fig. 5).

In a timing comparison in a fully uncontracted basis set, the GvFMM became as much as 50 times faster than analytic integration for fairly small-size molecular systems. All results reported in this paper were obtained with contracted bases, because these are commonly used in practical calculations. These results, although limited to benchmark graphene-sheets, are also valid for more complex materials. Given the speed, accuracy, and scaling properties of the GvFMM in practical, high-accuracy calculations, this method appears very promising for future electronic structure calculations on large molecular systems.

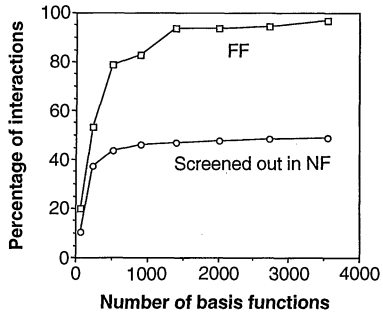

Fig. 5. (□) Percentage of interactions (uncontracted two-electron integrals) included in the FF component of the GvFMM (for the optimum box-size distribution used in Fig. 2) and treated by the tree hierarchy. (○) Percentage of uncontracted two-electron integrals that were prescreened and neglected in the NF portion of the Coulomb problem using empirical and mathematical bounds.

REFERENCES AND NOTES

1. L. Greengard, *Science* **265**, 909 (1994); _____ and V. Rokhlin, *J. Comput. Phys.* **73**, 325 (1987).
2. L. Greengard, *The Rapid Evaluation of Potential Fields in Particle Systems* (MIT Press, Cambridge, MA, 1988).
3. C. A. White and M. Head-Gordon, *J. Chem. Phys.* **101**, 6593 (1994); H. Ding, N. Karasawa, W. A. Goddard III, *ibid.* **97**, 4309 (1992); J. Shimada, H. Kaneko, T. Takada, *J. Comput. Chem.* **15**, 28 (1994).
4. C. A. White, B. G. Johnson, P. M. W. Gill, M. Head-Gordon, *Chem. Phys. Lett.* **230**, 8 (1994).
5. H. G. Petersen, D. Soelvason, J. W. Perram, E. R. Smith, *J. Chem. Phys.* **101**, 8870 (1994); *Proc. R. Soc. London Ser. A* **448**, 389 (1995).
6. S. F. Boys, *Proc. R. Soc. London Ser. A* **200**, 542 (1950).
7. The technical details of our present implementation, and an extensive study of the method's accuracy and speed, will be reported elsewhere. We prefer the name "Gaussian FMM" over "continuous FMM" [as in (*4*)] to underscore the fact that (i) the product of two Gaussian orbitals is a sum of well-localized Gaussian charge distributions amenable to efficient treatment by FMM, which is not true for other continuous charge distributions, and (ii) the error bound discussed here derives from and applies exclusively to Gaussian distributions.
8. Gaussian 95, Development version; M. J. Frisch *et al.*, Gaussian, Inc., Pittsburgh, PA.
9. D. L. Strout and G. E. Scuseria, *J. Chem. Phys.* **102**, 8448 (1995).
10. P. M. W. Gill and J. A. Pople, *Int. J. Quantum Chem.* **40**, 753 (1991).

11. This work was supported by the Air Force Office of Scientific Research (grant F49620-95-1-0203), the National Science Foundation (CHE-9321297), the Welch Foundation, and Gaussian, Inc. G.E.S. is a Camille and Henry Dreyfus Teacher-Scholar.

22 August 1995; accepted 30 October 1995

Low-Compressibility Carbon Nitrides

David M. Teter and Russell J. Hemley

First-principles calculations of the relative stability, structure, and physical properties of carbon nitride polymorphs predict a cubic form of C_3N_4 with a zero-pressure bulk modulus exceeding that of diamond. Like diamond, this new phase could potentially be synthesized at high pressure and quenched to ambient pressure for use as a superhard material. The calculations also predict that α-C_3N_4 and graphite-C_3N_4 are energetically favored relative to β-C_3N_4 and that published diffraction data can be re-indexed as α-C_3N_4 with lower error.

Intense theoretical and experimental interest has been focused on the possibility of new low-compressibility materials with bulk moduli and hardness exceeding that of diamond. Carbon nitrides have been proposed as superhard materials on the basis of empirical systematics (*1*). First-principles calculations have suggested that a hypothetical material, β-C_3N_4, may have a bulk modulus somewhat lower than that of diamond (*2, 3*). These results have motivated theoretical calculations (*4–8*) and experimental efforts to synthesize and characterize this compound (*10–20*). Amorphous C-N films have been synthesized (*14, 16, 20*), and small crystallites have been found in some of these films (*15, 17–19*). Electron diffraction patterns of these crystallites were indexed as the β-C_3N_4 structure. However, these data can also be fit to carbon phases (9). Other forms of carbon nitride with high hardness have been suggested, including a fullerene-like carbon nitride (*21*) and a crystalline carbon nitride composite (*22*). In this report, we investigate the stability and properties of carbon nitrides using first-principles calculations and show that α-C_3N_4 and graphite-C_3N_4 are energetically preferred over β-C_3N_4 and describe a cubic form of C_3N_4 that may have a zero-pressure bulk modulus (K_0) exceeding that of diamond and be metastable at zero pressure.

Assuming that a low-energy carbon nitride structure with a high bulk modulus must have carbon four-coordinated with nitrogen, and nitrogen three-coordinated with carbon, we have identified several additional prototype structures by considering chemical systems with this type of bonding topology and by locating dense structures in these systems. Using first-principles pseudopotential total energy techniques (*23*), we examined a series of C_3N_4 polymorphs to determine their energetics, structure, and physical properties, including K_0, density, and band gap.

Our calculations, like those in earlier studies of carbon nitride (*4–7*), were carried out using density-functional techniques within the local density approximation (LDA) to electron exchange and correlation. We used a preconditioned conjugate-gradient method to minimize the electronic degrees of freedom. The electronic wave

D. M. Teter, Geophysical Laboratory and Center for High Pressure Research, Carnegie Institution of Washington, Washington, DC 20015, USA, and Department of Materials Science and Engineering, Virginia Tech, Blacksburg, VA, 24061, USA.
R. J. Hemley, Geophysical Laboratory and Center for High Pressure Research, Carnegie Institution of Washington, 5251 Broad Branch Road, NW, Washington, DC, 20015, USA.